Quantum pBac: An effective, high-capacity *piggyBac*-based gene integration vector system for unlocking gene therapy potential

Wei-Kai Hua[1,*], Jeff C. Hsu[1,*], Yi-Chun Chen[1,*], Peter S. Chang[1], Kuo-Lan Karen Wen[1], Po-Nan Wang[2], Yi-Shan Yu[1], Ying-Chun Chen[1], I-Cheng Cheng[1], Sareina Chiung-Yuan Wu[1,†]

[1]GenomeFrontier Therapeutics, Inc. Taipei City, Taiwan (R.O.C.)

[2]Division of Hematology, Chang Gung Medical Foundation, Linkou Branch, Taipei City, Taiwan (R.O.C.)

*These authors contributed equally

†To whom correspondence may be addressed. Sareina Chiung-Yuan Wu; 18F-1, No. 3, Park St., Nangang Dist., Taipei City 11503, Taiwan (R.O.C.); +886-2-26558766;

Email: sareina@genomefrontier.com

Author Contributions: S.C.-Y.W. designed research. Y.-C.C., P.-N.W., Y.-S.Y., Y.-C.C., I.-C.C. performed research. W.-K.H., Y.-C.C, J.C.H., K.-L.K.W., and S.C.-Y.W. analyzed data. J.C.H., P.S.C. and S.C.-Y.W. wrote the paper.

Competing Interest Statement: S.C.-Y.W. is a founder of GenomeFrontier Therapeutics, Inc., W.-K.H., Y.-C.C., K.-L.K.W., Y.-S.Y., Y.-C.C., I.-C.C., and J.C.H. are affiliated with GenomeFrontier Therapeutics, Inc.

Classification: Biological Sciences, Medical Sciences.

Keywords: gene therapy | transposon | *piggyBac* | CAR-T

This PDF file includes:

Main Text
Figures 1 to 7

Abstract

Recent advances in gene therapy have brought novel treatment options to multiple fields of medicine, including cancer. However, safety concerns and limited payload capacity in commonly-utilized viral vectors prevent researchers from unlocking the full potential of gene therapy. Virus-free DNA transposons, including *piggyBac*, have been shown to obviate these shortcomings. We have previously demonstrated the superior transposition efficiency of a modified *piggyBac* system in HEK293 cells. Here, we further advanced and broadened the therapeutic application of this modified *piggyBac* system. We demonstrated that the internal domain sequence (IDS) within the 3' terminal repeat domain of hyperactive *piggyBac* (*hyPB*) donor vector contain dominant enhancer elements. We showed that a plasmid-free donor vector having IDS-free terminal inverted repeats in conjunction with a helper plasmid expressing *Quantum pBase*™ v2 form the most optimal *piggyBac* system, *Quantum pBac*™ (*qPB*), in T cells. We further demonstrated that T cells transfected with *qPB* expressing CD20/CD19 CAR outperformed cells transfected with the same donor vector but with plasmid expressing *hyPB* transposase in CAR-T cell production. Importantly, we showed that *qPB* produced mainly $CD8^+$ CAR-T cells that are also highly represented by T_{SCM}. These CAR-T cells effectively eliminated CD20/CD19-expressing tumor cells *in vitro* and in Raji-bearing immunodeficient mice. Our findings confirm that *qPB* is a promising virus-free vector system that is safer, and highly efficient in mediating transgene integration with the payload capacity to incorporate multiple genes.

Significance Statement

An effective, high capacity and safe gene integration vector system is critical to the success of gene therapy. We have previously modified a virus-free *piggyBac* transposon vector system and demonstrated its potential application in gene therapy. Here we further demonstrate that shortening of the *piggyBac* donor vector terminal repeat domain and backbone, coupled with *Quantum pBase*™ (*qPBase*) *v2*, result in the most optimal *Quantum pBac*™ (*qPB*) *piggyBac* system in human T cells. *qPBase v2* outperformed hyperactive *piggyBac* transposase in chimeric antigen receptor T (CAR-T) production. *qPB* produced CAR-T cells that are mainly $CD8^+$, highly represented by T_{SCM}, and effectively eliminated tumors *in vivo*. Our findings solidify *qPB* as a promising virus-free vector system for therapeutic application.

Main Text

Introduction

It has been well documented that almost all human diseases occur due to genetic defects. Gene therapy is the administration of genetic materials (i.e. DNA or RNA) to alter the biological properties of living cells for treating diseases(1). Thus, theoretically, gene therapy has the potential to cure most, if not all, diseases via a single treatment. Building upon decades of scientific, clinical, and manufacturing advances, gene therapy is now bringing novel treatment options to multiple fields of medicine, including cancer and genetic disorders.

Gene therapy often requires stable, long-term expression of therapeutic transgene(s) in cells. This is accomplished by engineering cells using viral or non-viral vector systems, either *ex vivo* or *in vivo*. Viral vectors are most commonly used for gene therapy due to their high efficiencies in gene delivery and integration, resulting in stable and long-term gene expression. However, viral vectors have several intrinsic limitations. These include (1) limited payload capacity that severely restricts the repertoire of genes that can be integrated(2); (2) genotoxicity arising from preferential integration into sites near or within active gene loci that may negatively impact the expression and/or function(s) of genes(3–8); (3) the proclivity of silencing genes introduced by viral vectors, presumably due to cellular immunity(9, 10); and (4) safety concerns related to immunogenicity of viral vectors(11). Additionally, production of viral vectors for clinical trials is costly, time consuming (> 6 months), and supply-constrained, which in turn represent a significant hurdle in routine medical practice(12).

In recent years, in conjunction with the technology advancement of non-viral gene delivery, virus-free DNA transposons have been shown to be capable of obviating these shortcomings and emerged as a promising vector system for gene therapy(13, 14), due to its effective gene integration capability(15). DNA transposons, also known as mobile elements or jumping genes, are genetic elements with the ability to transverse in the genome via a “cut-and-paste” mechanism. In nature, a simple DNA transposon contains a transposase gene flanked by terminal repeat sequences. During the transposition process, the ability of transposase to act *in trans* on virtually any DNA sequence that is flanked by the terminal repeat sequences makes DNA transposons particularly attractive as gene delivery tools for gene therapy. To turn DNA transposon into a tool for genetic engineering, a controllable bi-component vector system consisting of (1) a helper plasmid expressing the transposase and (2) a donor plasmid with exogenous DNA of interest flanked by the transposon terminal repeat sequences, was developed. Currently, *Sleeping Beauty* and *piggyBac* have been identified as the most promising DNA transposons for human gene therapy and have been clinically explored as vectors for several CAR-T cell therapies. Unlike *Sleeping Beauty* which was reconstructed from salmon

genome(16, 17), *piggyBac* derived from the cabbage looper moth *Trichoplusia ni* is naturally active in humans(18–20). By introducing amino acid mutations to the transposase, a *hyPB* transposase, *hyPBase*, and two hyperactive transposases of *Sleeping Beauty*, SB100X and hyperactive SB100X (30% more active than SB100X) were developed(21–25). When exogenous gene is *ex vivo* delivered to primary human T cells, *hyPBase* increased gene delivery rate by two to three folds, compared with *piggyBac* and SB100X transposases. Previously, by shortening of the *piggyBac* terminal repeat domain (TRD) sequences, we have observed a 2.6-fold increase in transposition activity mediated by *piggyBac* in HEK293 cells(26). We have also demonstrated that *hyPBase* activity can be further improved by two to three folds after fusing *hyPBase* with various peptides(27). In this study, we address whether the *piggyBac* system can be further developed for therapeutic application. We demonstrate that *qPB*, a binary *piggyBac* system comprising a plasmid-free donor vector and a helper plasmid expressing *Quantum pBase*™ (*qPBase*) *v2*, a molecularly-engineered *hyPBase*, is a simple yet robust and potentially safest vector system for generating potent CD19/CD20 dual-targeting CAR-T cells for treatment of B cell malignancies.

Results

Micro-*piggyBac* possesses significantly lower enhancer activity compared to mini-*piggyBac*

Malignancies caused by vector-mediated insertional activation of proto-oncogenes was evident in the initial clinical trial of retrovirus-based gene therapy for SCID-X1. The currently available minimal *piggyBac* transposon vector, designated as mini-*piggyBac* here, is composed of *cis* elements 5' (244 bp) and 3' (313 bp) TRD, which are transposed along with gene of interest into the genome. Each TRD contains a TIR sequence and an internal domain sequence (IDS). To minimize the potential risk of insertional mutagenesis caused by gene delivery vectors in gene therapy, we had previously generated micro-*piggyBac*, which contains the 5' (40 bp) and 3' (67 bp) TIR sequences of mini-*piggyBac*, while the respective IDS were removed.[26] However, it remains unclear whether the TRDs of mini-*piggyBac* and/or TIRs of micro-*piggyBac* harbor enhancer and/or silencer activity. To address this issue, a panel of luciferase reporter constructs containing individual TRD or TIR sequence was generated and examined for their luciferase activities in insect Sf9 cells, human HEK293 cells, and human Jurkat T cells (Figure 1). Compared to the control (construct **a**), the 3' TRD of mini-*piggyBac* (construct **c**) but not 3' TIR of micro-*piggyBac* (construct **e**) produced significantly higher luciferase activity across all three cell types (Figure 1B-1D), suggesting that enhancer activity is present in the 3' IDS of mini-*piggyBac*. On the other hand, a slight yet significantly-enhanced luciferase activity was detected in 5' TIR of

micro-*piggyBac* but not 5' TRD of mini-*piggyBac* in both HEK293 and Jurkat cells. This suggests the presence of a minimal level of enhanced activity in the 5' TIR and/or silencer activity in the 5' IDS of TRD (Figure 1B-1D). Taken together, micro-*piggyBac* possesses significantly lower enhancer activity compared to mini-*piggyBac*.

Shortening of donor vector backbone in combination with *Quantum pBase*™ (*qPBase*) *v2* enhances the transposition activity of micro-*piggyBac* in T cells

The significantly-reduced enhancer activity of TIRs suggests that micro-*piggyBac* is much safer for gene therapy applications. We therefore focused on micro-*piggyBac* and determined whether its transposition activity may be further enhanced by shortening the donor vector backbone, that is sequences outside of the TIR-spanning region. We constructed two donor vectors named micro-*piggyBac*-Short and micro-*piggyBac*-Long. Both of these vectors contain TIRs (micro) and either retains in its backbone the replication components, namely replication origin and antibiotic genes (Long), or is devoid of them (Short). A third donor vector, mini-*piggyBac* Long, which contains TRDs (mini) and retains the replication components in its backbone (Long), was also constructed for comparison since its combination with helper plasmid expressing *hyPBase* (commonly collectively referred to as "hyperactive *piggyBac*" or "*hyPB*") is currently the most advanced *piggyBac* system available (Figure 2A). We determined and compared the transposition efficiency of these donor vectors used in combination with helper plasmids expressing wild type *PBase* (pCMV-Myc-*PBase*), *hyPBase* (pCMV-HA-*hyPBase*), and *qPBase v1* or *v2* (pCMV-*qPBase_v1* and pCMV-*qPBase_v2*, respectively; Figure 2A).

As shown, *hyPBase*, either in combination with mini-*piggyBac*-Long or micro-*piggyBac*-Short or -Long, mediated markedly-enhanced transposition compared to *PBase* in T cells but not in HEK293 cells. *qPBase* v1, on the other hand, mediated markedly-enhanced transposition compared to *hyPBase* in HEK293, but not so much in T cells (Figure 2B-2D). These results suggest that the transposition activity of *hyPBase* and *qPBase v1* are likely cell type-dependent. We also found that *qPBase v2* mediated the highest transposition activity in almost all of the tested combinations and cell types. Importantly, when *qPBase v2* is accompanied by micro-*piggyBac*-Short donor vector, its transposition activity is by far the highest in both Jurkat and primary T cells and is clearly superior to *hyPBase* in combination with mini-*piggyBac*-Long, that is *hyPB piggyBac* system (Figures 2C and 2D, respectively).

Micro-*piggyBac* is superior to mini-*piggyBac* for advancing adeno-*piggyBac* hybrid vector for gene therapy

Even though *piggyBac* is capable of integrating sizable DNA (> 100 Kb), its genome engineering efficiency is largely restricted by the effectiveness of gene delivery methods.

Electroporation is an effective virus-free gene delivery method commonly used in gene therapy, but transfection efficiency is inversely correlated with the size of DNA delivered due to elevating cell damages caused by introduction of larger transgenes. Thus, to alleviate electroporation-associated restriction imposed on the *piggyBac* system, an adenovirus-*piggyBac* hybrid system, Ad-iPB7 was developed(28). Since the adenovirus genome exists in a linear form, here we also examined the transposition activity of linearized forms of mini-*piggyBac*-Long, micro-*piggyBac*-Short and micro-*piggyBac*-Long along with either *qPBase v1* or *qPBase v2* to gain insights for future development of adenovirus-*piggyBac* hybrid vector in gene therapy. As shown in Figure 2E, both micro-*piggyBac*-Short and micro-*piggyBac*-Long are superior compared to mini-*piggyBac*-Long. Moreover, when linearized micro-*piggyBac*-Long donor vector was combined with *qPBase v2*, a significantly greater transposition efficiency was observed compared to that produced when *qPBase v1* transposase was used (Figure 2E).

Minicircle micro-*piggyBac* is significantly more active than its parental counterpart in both Jurkat and primary T cells

Minicircle forms of DNA constructs offer several advantages, including enhancements in gene delivery efficiency and stable transgene expression. These advantages are due to the markedly reduced vector size of minicircle DNA as well as the lack of both antibiotic resistant genes and gene silencing induced by bacterial backbone sequences required for plasmid replication. We demonstrate that removal of these backbone sequences outside of the TIR-spanning regions via a cloning procedure (which shortens the size of the vectors) enhanced transposition efficiency (Figure 2). Therefore, we next used the Mark Kay minicircle system to generate a minicircle form of the donor vector (Q-tdTomato-IRES-hygro) from its parental plasmid counterpart (pQ-tdTomato-IRES-hygro) (Figure 3A)(29). We determined whether donor vector produced using minicircle technology will result in enhanced transposition efficiency similar to that produced by donor vectors with backbone replication components removed by molecular cloning.

When donor vectors of parental plasmid (pQ-tdTomato-IRES-hygro) and minicircle (Q-tdTomato-IRES-hygro) forms were compared, it was clear that minicircle donor vector mediated markedly higher transposition efficiency than its parental plasmid form, irrespective of the helper plasmid being co-electroporated. Moreover, only cells co-electroporated with minicircle donor vector and helper plasmid expressing *qPBase v2* consistently exhibited significantly higher transposition activity compared to all other combinations, including those with the helper plasmid expressing *hyPBase*. Based on these data in both Jurkat (Figure 3B) and primary T cells (Figure 3C), we selected micro-*piggyBac* vector in minicircle DNA form as the donor vector and a series of recombinant *qPBase* (*qPBase v1* and *v2*) as the helper plasmid to form the *Qunatum pBac*™ (*qPB*) system (Figure 3D).

When combined with CD20/CD19 CAR *Qunatum pBac*™ (*qPB*) donor vector, *Quantum pBase*™ (*qPBase*) *v2* outperforms *hyPBase* in CAR-T production

We next evaluated the performance of *qPB* system using anti-CD20/CD19 CAR as the transgene cassette of *qPB* donor vector with helper plasmid that encodes either *hyPBase* or *qPBase v2*. (Figure 4A).

The viability of cells electroporated with CD20/CD19 CAR *qPB* donor vector and helper plasmid expressing either *hyPBase* or *qPBase v2* were not significantly different one day after electroporation (Figure 4B). On the other hand, cells electroporated with helper plasmid expressing *qPBase v2* resulted in significantly more CAR^+ cells than those electroporated with helper plasmid expressing *hyPBase* on day 1 after nucleofection (Figure 4C, left panel). This difference was further amplified after 10 days of culture (Figure 4C, right panel), suggesting that the transposition efficiency of *qPBase v2* is much higher than that of *hyPBase*. Moreover, the expansion of cells electroporated with CD20/CD19 CAR *qPB* donor vector and helper plasmid expressing *qPBase v2* was also significantly higher than that of cells electroporated with the same donor vector but with helper plasmid expressing *hyPBase* (Figure 4D). These observations suggest that the transposition efficiency of *qPBase v2* is much higher than that of *hyPBase*.

***Qunatum pBac*™ (*qPB*) system produces CAR^+ T cells that are mainly of the $CD8^+$ subtype and are highly represented by the T_{SCM} subset**

Next, we analyzed T cells derived from six healthy donors to determine whether there may be donor-dependent variations in CAR^+ cell production using the *qPB* system (*qPB* donor vector with *qPBase v2* helper plasmid). The average percentage of CAR^+ T cells significantly increased from day 1 to 14 following electroporation (Figure 5A), with only one of six donors (donor 6) exhibiting a decrease in percentage of CAR^+ T cells. Fourteen days after electroporation, the percentage of $qPBase^+$ cells decreased to minimal levels (< 0.4 %) in all of the donors (Figure 5B), suggesting successful clearance of unwanted helper plasmids from T cells following completion of "cut-and-paste" gene-integration function. There was high variability among the PBMC donors (27-248 fold) in terms of the extent of CAR^+ T cell expansion during the 12-day culture period (Figure 5C), indicating a donor-dependent effect associated with the expansion capacity of these cells. We also profiled the T cell subtypes ($CD4^+$ and $CD8^+$; Figure 5D) as well as T cell subsets based on differentiation stages (Figure 5E, 5F) of CAR^+ T cells derived from the PBMC donors. $CD8^+$ T cells were the major T cell subtype population (Figure 5D). Furthermore, T_{SCM} was the major CAR^+ T cell subset in both CD4 and CD8 populations (Figure 5E, 5F).

Qunatum pBac™ (*qPB*) system produces functional CAR$^+$ T cells that kill target cells *in vitro*

We next determined whether CAR-T cells generated using the *qPB* system (*qPB* donor vector with *qPBase v2* helper plasmid) are functional in an *in vitro* setting. As shown in Figure 6A, compared to pan-T cells, CD20/CD19 dual-targeting CAR-T cells eradicated more CD19$^+$CD20$^+$ Raji cells (third row) and K562 target cells engineered to express either CD19 (first row), or CD20 (second row). On the other hand, CD20/CD19 dual-targeting CAR-T cells failed to eradicate BCMA (irrelevant antigen)-expressing control K562 cells (fourth row). These results demonstrated that the CAR-T cells specifically target and kill both CD20- and CD19-expressing cells. The cytotoxic functions of CAR-T cells from two donors (donor 1 and 2) were further assessed at different E:T ratios against Raji cells. We observed dose- and time-dependent killing by CAR-T cells derived from both donors (Figure 6B). Donor 2 CAR-T cells were markedly more potent in killing Raji cells, which is consistent with the higher level of IFN-γ detected in the 48-hour culture medium of donor 2 CAR-T cells compared with that of donor 1 CAR-T cells (Figure 6D). Notably, 74% of Raji cells were killed by donor 2 CAR-T cells after a 96-hour co-culture period even at a E:T ratio of 1:10 (Figure 6B). This is in contrast to the 15.5% killing of Raji cells by donor 1 CAR-T cells at the same E:T ratio, these results suggest a higher level of persistence in CAR-T cells derived from donor 2 as compared with those from donor 1. Supporting this notion, the percentages of CAR$^+$ T_{SCM} were higher in donor 2 (74.4% and 81.7% for CD4$^+$ and CD8$^+$ cells, respectively) compared to donor 1 (52.1% and 48.3% for CD4$^+$ and CD8$^+$ cells, respectively; Figure 6C).

Effective tumor clearance by *Qunatum pBac*™ (*qPB*)-generated CAR-T cells in Raji-bearing immunodeficient mice

Next, we tested the anti-tumor potency of donor 1 and donor 2 CAR-T cells in Raji-bearing immunodeficient mice (Figure 7A). Similar to the *in vitro* cytotoxicity results, Raji-bearing mice injected with low, medium and high doses of donor 1 CAR-T cells for five days killed Raji tumor cells in a dose-dependent fashion, where Raji tumors were completely eradicated by Day 5 and Day 9 in mice injected with high and medium doses of donor 1 CAR-T cells, respectively (Figure 7B). Consistent with this finding, Raji-bearing mice injected with medium dose of donor 2 CAR-T cells also eradicated Raji tumor cells. Moreover, in agreement with the greater *in vitro* cytotoxicity observed in donor 2 CAR-T cells (Figure 6), the Raji tumor killing also appeared to have occurred at an earlier time point (at Day 5 following CAR-T cell injection) compared with that of donor 1 CAR-T cells (at Day 9 following CAR-T cell injection).

Discussion

Sleeping Beauty (SB) and *piggyBac* (PB) are two DNA transposons that have been clinically explored recently for gene and cell therapy(15, 30). In addition to the multiple advantages over viral vectors mentioned earlier, the PB transposon system has the added benefits of (1) a large cargo capacity (> 100 kb)(31), (2) low frequency of footprint-induced mutations caused by integrant remobilization(32–34), (3) being perhaps the most active transposon system in human cells(35), and (4) being the most flexible transposon system amenable for a molecularly engineered transposase to retain activity, which greatly facilitate the potential site-specific genomic integration. These unique features also make *piggyBac* a superior gene therapy vector over *Sleeping Beauty*. Nevertheless, *Sleeping Beauty* has been considered to have less genotoxicity than *piggyBac* due to the following two concerns associated with *piggyBac*. First, *piggyBac*-like terminal repeat elements are prevalent in the human genome(36). Second, unlike a far more random genome integration profile of *Sleeping Beauty*, the genome integration profile of *piggyBac* is associated with euchromatin but excluded from heterochromatin(37, 38). This integration profile raises safety concerns since insertional mutagenesis of retroviral vector, which was found to be due to activation of the proto-oncogene LMO2 by the enhancer element of the retroviral integrant, was evident in three patients enrolled in the initial SCID-X1 clinical trial.

The abovementioned first safety concern of *piggyBac* system was thoroughly evaluated(39). The study demonstrated that expression of the transposase alone revealed no mobilization of endogenous *piggyBac*-like sequences in human genome and no increase in DNA double-strand breaks. Also, no selective growth advantage of *piggyBac*-harboring cells was found in long-term culture of primary human cells modified with eGFP-transposons(39). To address the abovementioned second concern related to potential tumorigenicity induced by enhancer activity of nearby integrants, we evaluated the enhancer activity of both mini- and micro-*piggyBac* and identified a significantly higher level of enhancer activity in the IDS region of 3' TRD in mini-*piggyBac*. Thus, by removing the IDS, our micro-*piggyBac* is expected to possess significantly lower enhancer activity, which in turn increases the safety profile of the donor vector. However, it has been well documented that both TIRs and other sequences contained in the TRDs are crucial for efficient integration of *piggyBac* transposon into the host genome. Several attempts to decrease the potential genotoxicity by reducing the size of the required TRDs to approximately 100 base pairs of TIRs resulted in significant losses in transposition efficiency(40–43). In contrast to these findings, our previous study demonstrated that by deleting IDS from both ends and leaving only TIRs (107 bp total in size), the transposition efficiency of *piggyBac* was increased by 2.6 fold in HEK293 when co-transfected with pPRIG-*piggyBac* which is a helper plasmid expressing a CMV promoter driving bi-cistronic transcript with myc-tagged wildtype

piggyBac transposase (*PBase*) and GFP linked by IRES26. However, in this study, we observed that the same truncated TRDs resulted in a two-fold reduction in transposition efficiency in HEK293, Jurkat, and human primary T cells when co-transfected with a different helper plasmid, a pcDNA 3.1 (control) vector with a CMV promoter that drives *PBase* expression (Figure 2). These observations suggest that the lowered transposition efficiency may be due to a suboptimal molar ratio of donor vector and the transposases that are being co-transfected. Interestingly, a marked increase in transposition efficiency can be observed in all cases when the cells were co-transfected with a helper plasmid expressing *qPBase v2*. This suggests that *qPBase v2* is the most robust and cell type-independent *piggyBac* transposase that can achieve the highest transposition activity irrespective of the type and configuration of the *piggyBac* donor vector. Furthermore, the genome-wide analysis of integration sites in HEK293 cells as shown in our previous study indicated that *qPBase v2* displayed a much more random integration profile with no detectable hot spots, and lower preference for CpG islands and cancer related genes as compared to that of *qPBase v1* and wildtype *piggyBac* transposase(27). Collectively, these observations suggest that micro-*piggyBac* in conjunction with *qPBase v2* should make a potentially safer *piggyBac* system.

In addition to the *cis* transposon sequences (TIRs) and *trans*-elements (transposase), the configuration of these *cis* and *trans* components can also highly impact the transposition efficiency, safety profile, and transgene stability. For example, to ensure the co-existence of the delivery cassette and transposase, a single plasmid transposon system was created which places TRDs within the delivery cassette, and the transposase gene in the helper part of the same plasmid(41). However, such an arrangement has the following disadvantages: (1) reduced rate of gene delivery due to an increase in size of DNA, a phenomenon particularly seen in electroporation-based gene delivery, (2) high degree of plasmid backbone DNA integration when using transposon plasmids(41), and (3) high rate of transposase integration(44). Given these disadvantages, the *trans*-configuration with two-plasmid system provides a safer and more effective transposon system.

However, the donor vector in a plasmid form has several undesirable qualities for clinical translation, including the presence of bacterial genetic elements and antibiotic-resistance genes. These undesirable risks exist because plasmid backbone integration from the transposon plasmid remains a possibility. Unmethylated CpG motifs highly enriched in the bacterial backbone of delivered plasmids have been shown to trigger strong inflammatory responses through toll-like receptor-9. These sequences will also induce transgene silencing, presumably, as a result of cellular immune response(45) and/or the induction of interferon(46). To reduce the chance of these events from occurring, a new *piggyBac* system was established by incorporating *piggyBac* transposon into a doggybone™ DNA (dbDNA) vector, which is a linear, covalently closed,

minimal DNA vector produced enzymatically *in vitro*(47). A recent report has demonstrated that dbDNA, which incorporates the *piggyBac* transposon system, can be used to generate stable CD19-targeting CAR-T cells at a similar efficiency level compared to its plasmid counterpart when a minimum of approximately 470 bp of additional randomly-selected DNA flanking the transposon is included. However, due to its linear configuration, db DNA should be less efficient for electroporation-based gene delivery as compared with its circular counterpart in supercoiled form. In this study, we adopted the Mark Kay minicircle technology to generate the smallest *piggyBac* transposon vector with TIRs (107 bp) and only 88 bp of the backbone sequence flanking the TIRs. This transposon donor vector in conjunction with *qPBase v2*, designated as Qunatum pBac™ (qPB), make the most superior *piggyBac* system that is minimalistic, highly efficient, and potentially safer (Figure 3).

We further demonstrated that the *qPB* system can be utilized to effectively generate CD19/CD20 dual-targeting CAR-T cells with 2-fold and 1.5-fold increases in the percentage of CAR^+ cells and expansion capacity, respectively, as compared to those utilizing *hyPBase* (Figure 4). Additionally, the CAR-T cell expansion and persistence emerged as key efficacy determinants in cancer patients and both are positively correlated with the proportion of T_{SCM} in the final CAR-T cell product(48, 49). We demonstrated potent *in vitro* and *in vivo* anti-tumor efficacies in *qPB*-derived CAR-T cells, which are dominated by the T_{SCM} population, especially in the $CD8^+$ CAR^+ T cells. Additionally, to minimize genotoxicity caused by transposase-induced integrant remobilization, transposase in a mRNA configuration has been adopted in transposon-based CAR-T clinical trials(50). However, as compared to transposase in DNA form, its mRNA counterpart is generally less efficient, more costly for GMP production, and less stable for storage. Given the low frequency of footprint-induced mutation by *piggyBac* (< 5 %) and the fact that only a minimal portion (< 0.4 %) of CAR^+ T cells expressed detectable level of *qPBase* in CAR-T cells (Figure 5B), transposase in a plasmid form should be sufficiently safe when applied to highly proliferative *ex vivo*-engineered cells. Additionally, our recent genome-wide integration profiling of *qPB* in CAR-T products derived from two distinct donors further support its safe use in T cell engineering(52).

In summary, given its large payload capacity, high level of efficiency, and outstanding safety profile, *qPB* is likely the most superior system suitable for the development of next generation virus-free gene and cell therapy, especially for development of multiplex CAR-T therapy.

Materials and Methods

Human T cell samples from healthy donors

Blood samples from adult healthy donors were obtained from Chang Gung Memorial Hospital (Linkou, Taiwan), the acquisition of these samples was approved by the Institution Review Board (IRB No. 201900578A3) at Chang Gung Medical Foundation.

Vector constructs

Plasmids were constructed following the protocols described previously (51) and are described briefly below. Minicircle DNA were purchased from Aldevron (Fargo, ND). All of the PCR products or junctions of constructs (wherever sequences are ligated) were confirmed by sequencing.

Vector construction

pGL3-miniP (Construct a; Figure 1A)

pGL3-basic is digested with SacI and HindIII. The CMV mini-promoter with SacI and HindIII sequences on its 5' and 3' ends, respectively was synthesized, double-digested with SacI and HindIII, and ligated to the SacI-HindIII vector fragment of pGL3-basic to make construct **a** as shown in Figure 1A.

Constructs b-e (Figure 1A)

pGL3-miniP was digested with KpNI and XhoI. The 5'TIR or 3'TIR of micro-*piggyBac* or 5'TRD or 3'TRD of mini-*piggyBac* with kpnI and XhoI sequences added on either end was synthesized, double-digested with KpnI and XhoI, and ligated to the KpnI-XhoI vector fragment of pGL3-miniP, respectively, to make the set of constructs (**b**-**e**) for evaluation of enhancer activity of mini-*piggyBac*'s and micro-*piggyBac*'s TRDs and TIRs, respectively.

Donor vectors (Figure 2A)

"Mini-*piggyBac*-Long" is the same construct as the donor of *piggyBac* system published previously (20)

"Micro-*piggyBac*-Short" is the plasmid named "*pPB*-cassette short" as published previously(26)

"Micro-*piggyBac*-Long" is constructed by replacing the backbone of "micro-*piggyBac*-Short" with that of "mini-*piggyBac*-Long" via PCR-based cloning.

Helper plasmid (Figure 2A)

The construction of helper plasmid was described previously(27).

Parental *qPB* donor vector (Figure 3A)

The parental plasmid contains the sequences of the following components (obtained by DNA synthesis) arranged in a 5' to 3' order: Kanamycin resistance gene, origin of replication (pMB1), 32 I-SceI sites, attB site (PhiC31), 5'TIR of micro-*piggyBac*, multiple cloning site (MSC), 3'TIR of micro-*piggyBac*, and attP (PhiC31).

pQ-tdTomato-IRES-hygro (Figure 3A)

The DNA for a cassette with the CAG promoter driving a bi-cistronic transcript containing td-tomato gene, internal ribosome entry site (IRES) of Foot-and-mouth disease virus (FMDV), and hygromycin resistance gene was synthesized and cloned into the AseI and EcoRV site of the parental *qPB* vector to make pQ-tdTomato-IRES-hygro.

pQ-CD20CD19CAR (Figure 4A)

The dual-targeting tandem CD20/CD19 CAR-containing pQ-CD20CD19CAR vector encodes an second-generation CAR composed by an elongation factor 1-alpha (EF1α) promoter linked (via a 2A element) to an extracellular domain derived from the single chain variable fragment (scFv) of monoclonal antibodies directed against the CD19 (FMC63) and CD20 (Leu16) antigens, respectively, and further linked to the CD3z chain of the TCR complex by means of a CD8 hinge and transmembrane domains, together with the 4-1BB co-stimulatory domain. Following synthesis, the expression cassette is cloned into the MCS of parental *qPB* vector to make pQ-CD20CD19CAR.

Minicircle DNA

The minicircle DNAs, Q-tdTomato-IRES-hygro (Figure 3A) and Q-CD20CD19CAR (Figure 4A), are manufactured by Aldevron from their parental plasmid, pQ-tdTomato-IRES-hygro and pQ-CD2019CAR, respectively.

qPBase

To comply with the FDA regulations, the ampicillin gene in the helper plasmid expressing *qPBase v2* was replaced by a kanamycin resistance gene sequence to make *qPBase. qPBase* combines with *qPB* donor vector (minicircle DNA) to form the *qPB* system.

Enhancer assay

The control, pPL-TK (Renilla Luciferase), was co-transfected with the specified firefly luciferase constructs (i.e., pGL3-miniP, pGL3-miniP-microL, pGL3-miniP-microR, pGL3-miniP-miniR, pGL3-miniP-miniL, mini-*piggyBac* Long, micro-*piggyBac* Short, or micro-*piggyBac* Long) by either Fugene (HEK293) or Nuclefection (Sf9 cells, and Jurkat T cells). In some experiments, constructs were first linearized utilizing a XmnI or Bgl I restriction enzyme. Forty-eight hours after transfection, cells were harvested and subjected to Dual-Luciferase assay (Promega) by following the manufacturing instructions.

Transposition assay

HEK293 cells (1×10^5) were transfected with 200-334 ng of donor vector carrying a hygromycin resistance gene and 200-282 ng of helper plasmid in MEM medium (GeneDireX), 10% FBS (Corning) utilizing the X-tremeGENE^{TM} HP DNA transfection reagent (Merck). Transfected cells

were transferred to 100-mm plates and cultured under hygromycin (100 ug/ml) selection pressure for 14 days. Cells were then harvested and fixed with 4% paraformaldehyde. Fixed cells were stained with 0.2% methylene blue and cell colonies were enumerated.

Jurkat or primary T cells (2 x × 10^5) were electroporated with 400-668 ng of donor vector carrying a hygromycin resistance gene which in some experiments was also linked to a tdTomato gene, and 400-517 ng of helper plasmid in OpTimizer medium supplemented with *Quantum Booster*™ (GenomeFrontier). Electroporation was carried out using a 4D-Nucleofector™ (Lonza) in combination with the *Quantum Nufect*™ Kit (GenomeFrontier) according to the manufacturer's instructions. Electroporated cells were transferred to 96-well plates and cultured under hygromycin (1 mg/ml) selection pressure for 14 days. Cells were then harvested and stained with AO/PI. Live cell numbers were determined using Celigo image cytometry (Nexcelom). Transposition efficiency was expressed as number of hygromycin-resistant colonies or live cells.

Generation and expansion of CAR-T cells

Peripheral blood mononuclear cells (PBMCs) were isolated from blood samples of healthy donors by utilizing Ficoll-Hypaque gradient separation. $CD3^+$ T cells were isolated from PBMCs using EasySep™ Human T Cell Isolation Kit (StemCell Technologies) according to the manufacturer's instructions. T cells were activated by co-incubation with Dynabeads™ (Invitrogen) in X-VIVO 15 medium (Lonza) for two days at a beads to cells ratio of 3:1. Following the removal of Dynabeads™, activated T cells were harvested and freezed or utilized in experiments. Electroporation of activated T cells was carried out using a Nucleofector™ 2b Device (Lonza) in combination with the *Quantum Nufect*™ Kit (GenomeFrontier) according to the manufacturer's instructions. Cells were electroporated with the combination of CD20/CD19 CAR donor vector, and pCMV-*hyPBase* or pCMV-*qPBase v2* helper vector. Cells were cultured and expanded for 10 or 14 days in OpTmizer medium (Thermo Fisher Scientific) supplemented with 50IU of IL-2 (PeproTech) and 10% FBS, and thereafter harvested for experiment. γ-irradiated aAPC were added on Day 3 to the T cell expansion cultures at a aAPC:T cell ratio of 1:1.

Evaluation of CAR-T cells performance

CAR expression on T cells was determined by flow cytometry analysis following staining of cells at 4℃ for 30 minutes with $F(ab')_2$ fragment specific, biotin-conjugated goat anti-mouse antibodies (Jackson ImmunoResearch Laboratories) and R-phycoerythrin (PE)-conjugated streptavidin (Jackson ImmunoResearch Laboratories). Similarly, cells were also stained with the following antigen-specific antibodies: CD3-Pacific Blue, CD4-Alexa Flour 532 (Thermo Fisher Scientific), CD8-PE-Cy7, CD45RA-BV421, CD62L-PE-Cy5, or CD95-BV711 (Biolegend). Cells may also be incubated with propidium iodide (PI, Thermo Fisher Scientific) and/or Acridine orange (AO,

Nexcelom). PI^- cells and T cell differentiation subsets were determined by flow cytometry based on CD45RA, CD62L and CD95 expression: T_N ($CD45RA^+CD62L^+CD95^-$), T_{SCM} ($CD45RA^+CD62L^+CD95^+$), T_{CM} ($CD45RA^-CD62L^+$), T_{EM} ($CD45RA^-CD62L^-$), and T_{EFF} ($CD45RA^+CD62L^-$). *qPBase* is expressed as a fusion protein of GFP and transposase. Its expression was determined by flow cytometry analysis of GFP^+ cells. In some experiments a hygromycin resistant gene was expressed with a tdTomato gene and hygromycin resistant cells was determined by flow cytometry analysis of $tdTomato^+$ cells. Flow cytometric measurements and analyses were performed on a SA3800 Spectral Analyzer (Sony). Histograms and dot-plots were generated using GraphPad Prism software (GraphPad). Live cells were determined using Celigo image cytometry (Nexcelom) and represent the number of AO^+, PI^- cells.

***In vitro* cytotoxicity assay**

Target antigen-expressing cells were engineered as according to the method described elsewhere(52). 5 x 10^3 cells per well of $CD19^+$ (K562 CD19-tdTomato), $CD20^+$ (K562 CD20-GFP), $CD19^+CD20^+$ (Raji-GFP) or non-relevant K562 BCMA-GFP target cells were seeded in 96-well culture plates (Corning) and control Pan-T or CAR-T cells were added at an E:T ratio of 5:1, 1:1, 1:3 or 1:10. CAR-T cells mediated cytotoxicity on target cells was then assessed by using Celigo image cytometry (Nexcelom) to determine the number of live target cells at 0, 24, 48, 72 and 96 hours after co-culturing. Cell aggregates were separated by pipetting before Celigo imaging. The percent specific lysis for each sample was calculated using the formula: [1-(live fluorescent cell count in the presence of target cells and CAR-T cells / live fluorescent cell count in the presence of target cells only)] x 100.

***In vitro* cytokine release assay**

Pan-T control cells or CAR-T cells produced from two volunteer donors were thawed and added to cultures containing $CD19^+$ (K562 CD19-tdTomato), $CD20^+$ (K562 CD20-GFP), $CD19^+CD20^+$ (Raji-GFP) or non-relevant K562 BCMA-GFP tumor target cells. The cells were added at an effector:target (E:T) ratio of 10:1 in OpTmizer medium supplemented with 50IU of IL-2 and 10% FBS. Following 48 h of co-culture, supernatant was collected and IFN-γ levels in the culture supernatant was measured by performing enzyme-linked immunosorbent assay (Thermo Fisher) according to the manufacturer's instructions.

Mouse xenograft model

In vivo studies using mouse xenograft model were conducted at the Development Center for Biotechnology, Taiwan, using animal protocols approved by the Taiwan Mouse Clinic IACUC (2020-R501-035). Briefly, eight-week-old female ASID (NOD.Cg-Prkdc^{scid}Il2rg^{tm1Wjl}/YckNarl) mice

(National Laboratory Animal Center, Taiwan) were intravenously (i.v.) injected with 1.5 x 10^5 Raji-Luc/GFP tumor cells. One week after Raji-Luc/GFP tumor cell injection, mice were injected with 3 x 10^6 CAR-T cells or control Pan-T cells. Luminescence signals from Raji-Luc/GFP tumor cells was monitored using the Xenogen-IVIS Imaging System (Caliper Life Sciences).

Statistical analysis

Statistical analyses of differences between two groups and among three or more groups were carried out using the Student's t-test (two-tailed) and the one-way ANOVA with Tukey's multiple comparison test, respectively. The analyses were performed using GraphPad Prism software (GraphPad Software), and statistical significance was reported as * $p < 0.05$, ** $p < 0.01$, and *** $p < 0.001$. Differences are considered to be statistically significant when $p < 0.05$.

Acknowledgments

The authors thank Ms. Lu-Chun Chen for her assistance throughout the IRB preparation and approval process. The authors also thank Dr. Pei-Yi Tsai for assistance with the animal experiments.

References

1. T. Strachan, A. Read, "Mapping Genes Conferring Susceptibility to Complex Diseases" in *Human Molecular Genetics*, (2020), pp. 467–496.

2. S. Ghosh, A. M. Brown, C. Jenkins, K. Campbell, Viral Vector Systems for Gene Therapy: A Comprehensive Literature Review of Progress and Biosafety Challenges. *Applied Biosafety* **25**, 7–18 (2020).

3. A. Nowrouzi, H. Glimm, C. von Kalle, M. Schmidt, Retroviral vectors: Post entry events and genomic alterations. *Viruses* **3**, 429–455 (2011).

4. A. R. W. Schröder, *et al.*, HIV-1 integration in the human genome favors active genes and local hotspots. *Cell* **110**, 521–529 (2002).

5. D. Cesana, *et al.*, Whole transcriptome characterization of aberrant splicing events induced by lentiviral vector integrations. *Journal of Clinical Investigation* **122**, 1667–1676 (2012).

6. U. Modlich, *et al.*, Insertional transformation of hematopoietic cells by self-inactivating lentiviral and gammaretroviral vectors. *Molecular Therapy* **17**, 1919–1928 (2009).

7. S. Hacein-Bey-Abina, *et al.*, Insertional oncogenesis in 4 patients after retrovirus-mediated gene therapy of SCID-X1. *Journal of Clinical Investigation* **118**, 3132–3142 (2008).

8. D. Cesana, *et al.*, Uncovering and dissecting the genotoxicity of self-inactivating lentiviral vectors in vivo. *Molecular Therapy* **22**, 774–785 (2014).

9. D. Jähner, R. Jaenisch, Retrovirus-induced de novo methylation of flanking host sequences correlates with gene inactivity. *Nature* **315**, 594–597 (1985).

10. D. Jähner, *et al.*, De novo methylation and expression of retroviral genomes during mouse embryogenesis. *Nature* **298**, 623–628 (1982).

11. S. E. Raper, *et al.*, Fatal systemic inflammatory response syndrome in a ornithine transcarbamylase deficient patient following adenoviral gene transfer. *Molecular Genetics and Metabolism* **80**, 148–158 (2003).

12. J. C. M. van der Loo, J. F. Wright, Progress and challenges in viral vector manufacturing. *Hum Mol Genet* **25**, R42–R52 (2016).

13. M. Ramamoorth, A. Narvekar, Non viral vectors in gene therapy - An overview. *Journal of Clinical and Diagnostic Research* **9**, GE01–GE06 (2015).

14. Y. J. J. Meir, S. C. Y. Wu, Transposon-based vector systems for gene therapy clinical Trials: Challenges and considerations. *Chang Gung Medical Journal* **34**, 565–579 (2011).

15. J. Tipanee, Y. C. Chai, T. vanden Driessche, M. K. Chuah, Preclinical and clinical advances in transposon-based gene therapy. *Bioscience Reports* **37**, BSR20160614 (2017).

16. Z. Ivics, P. B. Hackett, R. H. Plasterk, Z. Izsvák, Molecular reconstruction of sleeping beauty, a Tc1-like transposon from fish, and its transposition in human cells. *Cell* **91**, 501–510 (1997).

17. Z. Ivics, Z. Izsvák, A whole lotta jumpin' goin' on: New transposon tools for vertebrate functional genomics. *Trends in Genetics* **21**, 8–11 (2005).

18. M. J. Fraser, G. E. Smith, M. D. Summers, Acquisition of Host Cell DNA Sequences by Baculoviruses: Relationship Between Host DNA Insertions and FP Mutants of Autographa californica and Galleria mellonella Nuclear Polyhedrosis Viruses. *Journal of Virology* **47**, 287–300 (1983).

19. S. Ding, *et al.*, Efficient transposition of the piggyBac (PB) transposon in mammalian cells and mice. *Cell* **122**, 473–483 (2005).

20. S. C. Y. Wu, *et al.*, piggyBac is a flexible and highly active transposon as compared to Sleeping Beauty, Tol2, and Mos1 in mammalian cells. *Proc Natl Acad Sci U S A* **103**, 15008–15013 (2006).

21. L. Mátés, *et al.*, Molecular evolution of a novel hyperactive Sleeping Beauty transposase enables robust stable gene transfer in vertebrates. *Nature Genetics* **41**, 753–761 (2009).

22. F. Voigt, *et al.*, Sleeping Beauty transposase structure allows rational design of hyperactive variants for genetic engineering. *Nature Communications* **7**, 11126 (2016).

23. J. Cadiñanos, A. Bradley, Generation of an inducible and optimized piggyBac transposon system. *Nucleic Acids Research* **35**, e87 (2007).

24. K. Yusa, L. Zhou, M. A. Li, A. Bradley, N. L. Craig, A hyperactive piggyBac transposase for mammalian applications. *Proc Natl Acad Sci U S A* **108**, 1531–1536 (2011).

25. K. Yusa, "piggyBac transposon" in *Mobile DNA III*, (ASM Press, 2015), pp. 873–890.

26. Y. J. J. Meir, *et al.*, Genome-wide target profiling of piggyBac and Tol2 in HEK 293: Pros and cons for gene discovery and gene therapy. *BMC Biotechnology* **11**, 28 (2011).

27. Y. J. J. Meir, *et al.*, A versatile, highly efficient, and potentially safer piggyBac transposon system for mammalian genome manipulations. *FASEB Journal* **27**, 4429–4443 (2013).

28. A. L. Cooney, B. K. Singh, P. L. Sinn, Hybrid nonviral/viral vector systems for improved piggyBac DNA transposon in vivo delivery. *Molecular Therapy* **23**, 667–674 (2015).

29. M. A. Kay, C. Y. He, Z. Y. Chen, A robust system for production of minicircle DNA vectors. *Nature Biotechnology* **28**, 1287–1289 (2010).

30. C. F. Magnani, *et al.*, Transposon-Based CAR T Cells in Acute Leukemias: Where are We Going? *Cells* **9**, 1337 (2020).

31. R. Li, Y. Zhuang, M. Han, T. Xu, X. Wu, PiggyBac as a high-capacity transgenesis and gene-therapy vector in human cells and mice. *DMM Disease Models and Mechanisms* **6**, 828–833 (2013).

32. T. A. Elick, Excision of the piggy Bac transposable element in vitro is a precise event that is enhanced by the expression of its encoded transposase. *Genetica* **98**, 33–41 (1996).

33. M. A. Li, *et al.*, The piggyBac Transposon Displays Local and Distant Reintegration Preferences and Can Cause Mutations at Noncanonical Integration Sites. *Molecular and Cellular Biology* **33**, 1317–1330 (2013).

34. Q. Chen, *et al.*, Structural basis of seamless excision and specific targeting by piggyBac transposase. *Nature Communications* **11**, 3446 (2020).

35. J. E. Doherty, *et al.*, Hyperactive piggybac gene transfer in human cells and in vivo. *Human Gene Therapy* **23**, 311–320 (2012).

36. C. Feschotte, The piggyBac transposon holds promise for human gene therapy. *Proc Natl Acad Sci U S A* **103**, 14981–14982 (2006).

37. D. L. Galvan, *et al.*, Genome-wide mapping of piggybac transposon integrations in primary human T cells. *Journal of Immunotherapy* **32**, 837–844 (2009).

38. M. Hamada, *et al.*, Integration Mapping of piggyBac-Mediated CD19 Chimeric Antigen Receptor T Cells Analyzed by Novel Tagmentation-Assisted PCR. *EBioMedicine* **34**, 18–26 (2018).

39. S. Saha, *et al.*, Evaluating the potential for undesired genomic effects of the piggyBac transposon system in human cells. *Nucleic Acids Research* **43**, 1770–1782 (2015).

40. X. Li, *et al.*, piggyBac internal sequences are necessary for efficient transformation of target genomes. *Insect Molecular Biology* **14**, 17–30 (2005).

41. V. Solodushko, V. Bitko, B. Fouty, Minimal piggyBac vectors for chromatin integration. *Gene Therapy* **21**, 1–9 (2014).

42. T. A. Elick, N. Lobo, M. J. Fraser, Analysis of the cis-acting DNA elements required for piggyBac transposable element excision. *Molecular and General Genetics* **255**, 605–610 (1997).

43. X. Li, N. Lobo, C. A. Bauser, M. J. Fraser, The minimum internal and external sequence requirements for transposition of the eukaryotic transformation vector piggyBac. *Molecular Genetics and Genomics* **266**, 190–198 (2001).

44. J. Urschitz, *et al.*, Helper-independent piggyBac plasmids for gene delivery approaches: Strategies for avoiding potential genotoxic effects. *Proc Natl Acad Sci U S A* **107**, 8117–8122 (2010).

45. Z. Y. Chen, *et al.*, Linear DNAs concatemerize in vivo and result in sustained transgene expression in mouse liver. *Molecular Therapy* **3**, 403–410 (2001).

46. S. Huerfano, B. Ryabchenko, J. Forstová, Nucleofection of expression vectors induces a robust interferon response and inhibition of cell proliferation. *DNA and Cell Biology* **32**, 467–479 (2013).

47. D. C. Bishop, *et al.*, CAR T Cell Generation by piggyBac Transposition from Linear Doggybone DNA Vectors Requires Transposon DNA-Flanking Regions. *Molecular Therapy - Methods and Clinical Development* **17**, 359–368 (2020).

48. L. Gattinoni, D. E. Speiser, M. Lichterfeld, C. Bonini, T memory stem cells in health and disease. *Nature Medicine* **23**, 18–27 (2017).

49. L. Biasco, *et al.*, Clonal expansion of T memory stem cells determines early anti-leukemic responses and long-term CAR T cell persistence in patients. *Nature Cancer* **2**, 629–642 (2021).

50. S. Prommersberger, *et al.*, CARAMBA: a first-in-human clinical trial with SLAMF7 CAR-T cells prepared by virus-free Sleeping Beauty gene transfer to treat multiple myeloma. *Gene Therapy* **28**, 560–571 (2021).

51. J. Sambrook, D. W. Russell, "Molecular Cloning: A Laboratory Manual, Third Edition" in *Molecular Cloning: A Laboratory a Manual,* (2001), pp. 1.32-1.34.

52. Y.-C. Chen, *et al.*, *Quantum CART* (*qCART*), a *piggyBac*-based system for development and production of virus-free multiplex CAR-T cell therapy (*Manuscript in preparation*).

Figures and Tables

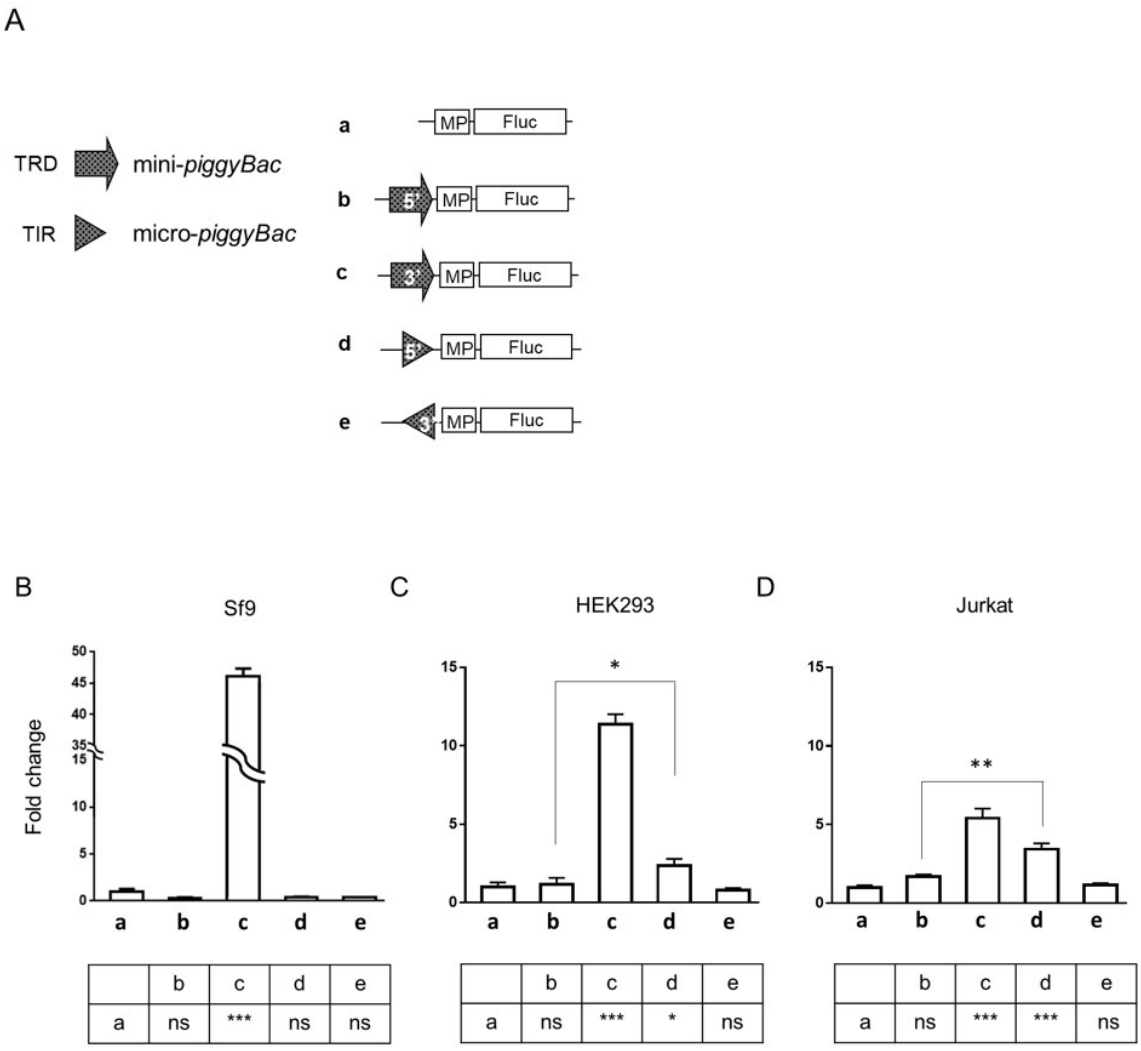

Figure 1. Enhancer/silencer activity of mini-*piggyBac* TRDs and micro-*piggyBac* TIRs

(A) A schematic depiction showing a panel of luciferase reporter constructs containing a CMV minimal promoter (MP) and firefly luciferase (Fluc) gene, with or without the 5' or 3' TRDs from mini-*piggyBac* or 5' or 3' TIRs from micro-*piggyBac* inserted upstream of MP. Luciferase activities exhibited by the reporter constructs of (A) in (B) Sf9, (C) HEK293, and (D) Jurkat cells. Results are shown as mean fold changes in luciferase activity ± standard deviation (SD; normalized first to Renilla luciferase activity and then to the luciferase activity obtained from cells transfected with construct a). Statistical analysis results of differences in fold change between luciferase activity obtained from cells transfected with construct **a** and those from cells transfected with constructs **b**-**e** are summarized in the lower panels (boxed regions). * $p < 0.05$, ** $p < 0.01$, *** $p < 0.001$. N = 3 (triplicates).

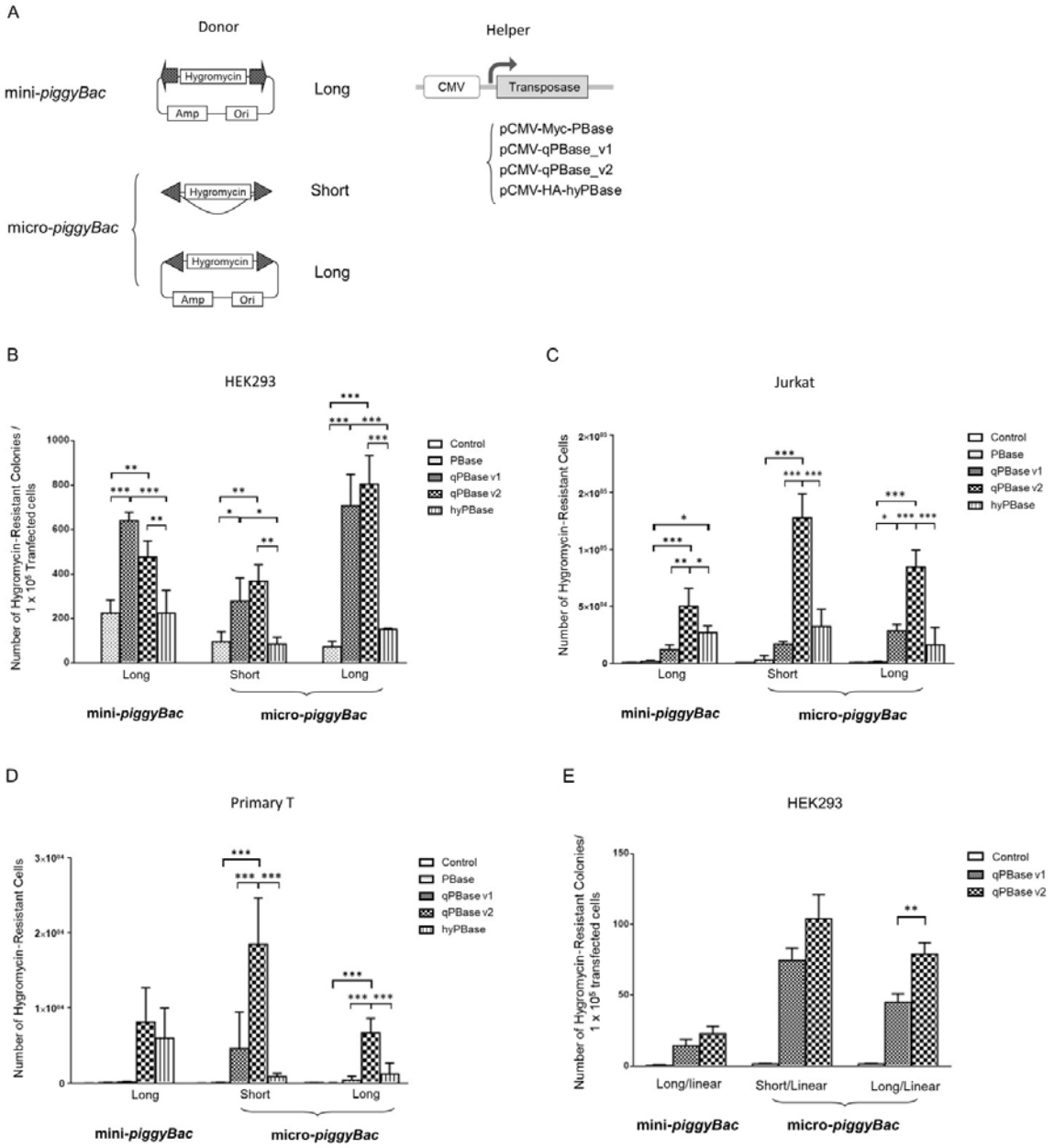

Figure 2. Transposition activity of various donor vector and helper plasmid combinations in human cells

(A) A schematic depiction showing the *piggyBac* system with various donor vectors and helper plasmids as indicated. Transposition activity of the indicated combination of donor vector and helper plasmid in (B) HEK293, (C) Jurkat, and (D) primary T cells. (E) Transposition activity of the indicated combination of linearized donor vector and helper plasmid in HEK293 cells. Results are shown as mean number of hygromycin-resistant colonies/1×10^5 transfected cells ± SD (B and E), and mean number of hygromycin-resistant cells ± SD (C and D). * $p < 0.05$, ** $p < 0.01$, *** $p < 0.001$. N = 3 (triplicates).

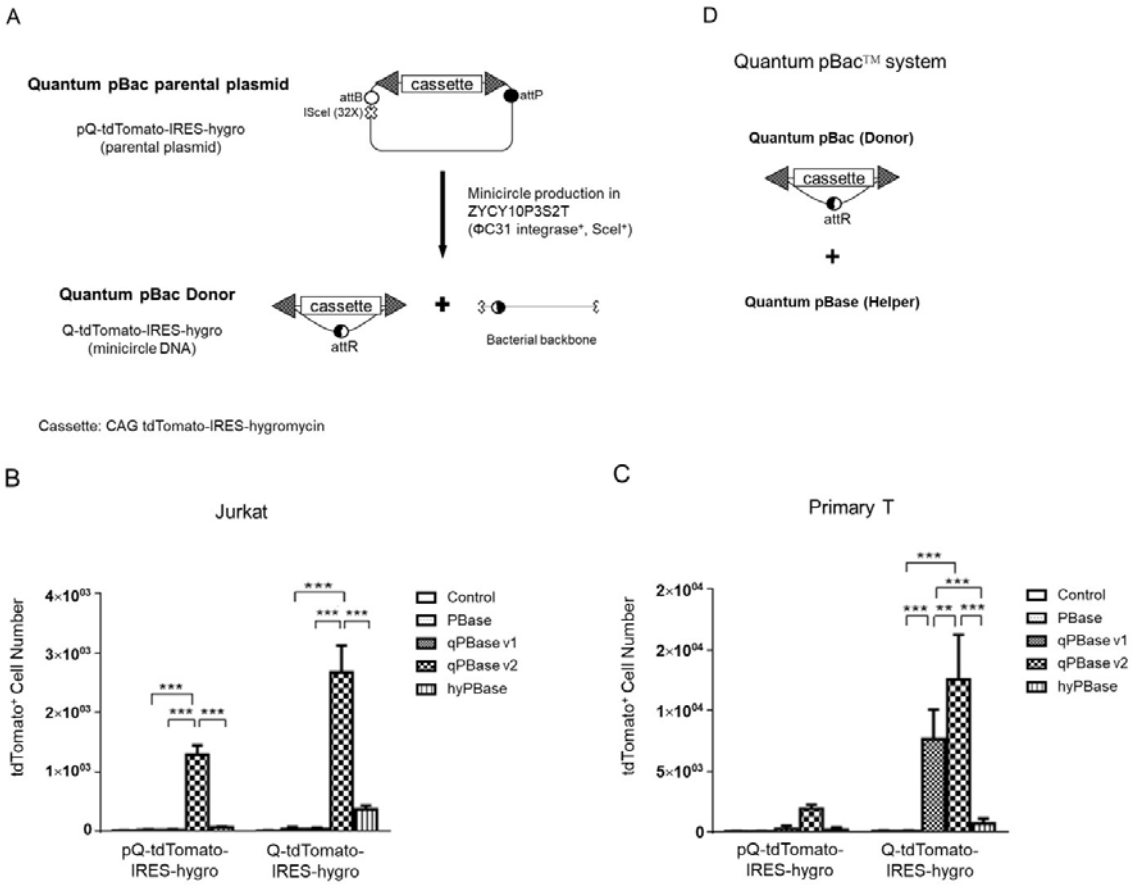

Figure 3. Transposition activity of various transposases with donor vector in parental plasmid or minicircle counterpart forms

(A) A schematic depiction illustrating the generation of the *Quantum pBac*™ (*qPB*) donor vector having a gene cassette carrying tdTomato and hygromycin genes linked by IRES (Q-tdTomato-IRES-hygro) from its parental plasmid (pQ-tdTomato-IRES-hygro). Transposition activity of the indicated combination of pQ-tdTomato-IRES-hygro or Q-tdTomato-IRES-hygro donor vector and helper plasmid in (B) Jurkat and (C) primary T cells. (D) A schematic depiction showing the two-components *qPB* system. Results are shown as mean number of tdTomato$^+$ cells ± SD. ** $p < 0.01$, *** $p < 0.001$. N = 3 (triplicates).

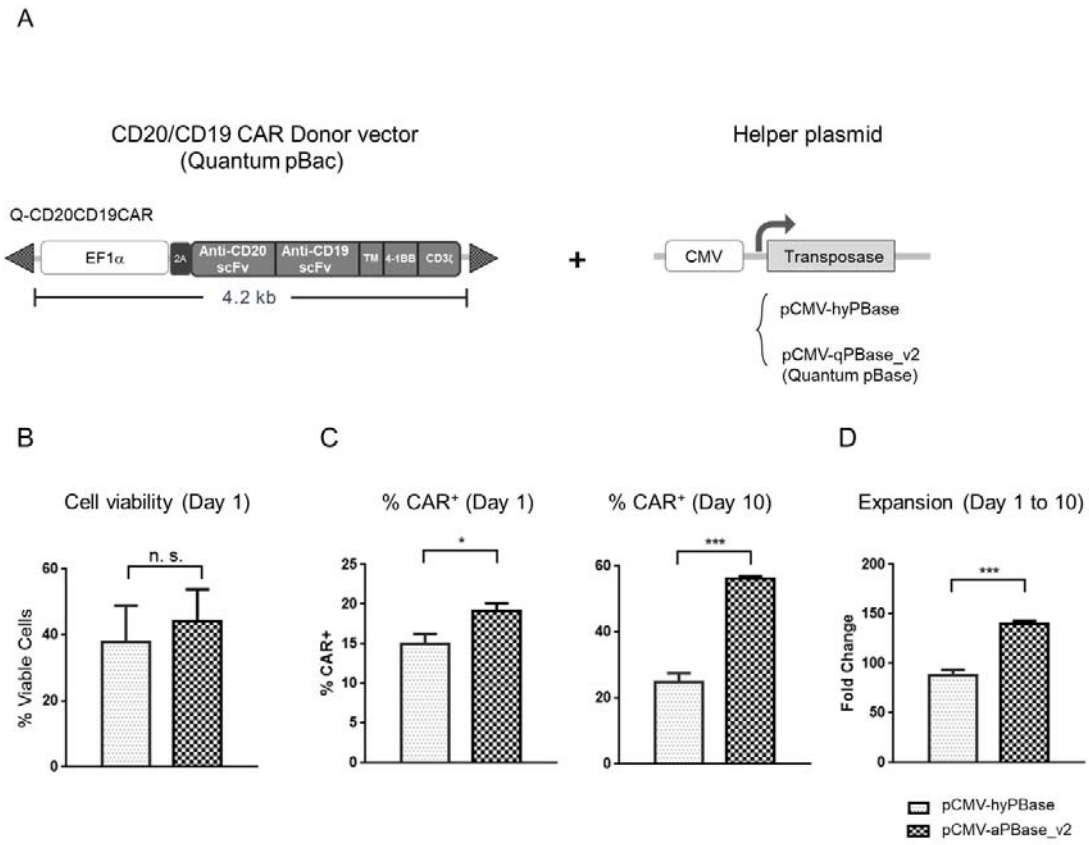

Figure 4. CAR-T cell production using *Qunatum pBac*™ (*qPB*) donor vector and helper plasmid

(A) A schematic depiction showing the CD20/CD19 CAR *qPB* donor vector and helper plasmid pCMV-*hyPBase* or pCMV-*qPBase_v2*. Characterization of (B) cell viability one day following electroporation, (C) percentages of CAR^+ cells on days 1 and 10 following electroporation, and (D) fold expansion of cells after 10 days of culture. Results are shown as mean percentage of viable cells ± SD (B), mean percentage of CAR^+ cells ± SD (C), and mean fold change ± SD (D). n.s. not statistically significant, * $p < 0.05$, *** $p < 0.001$. N = 3 (triplicates).

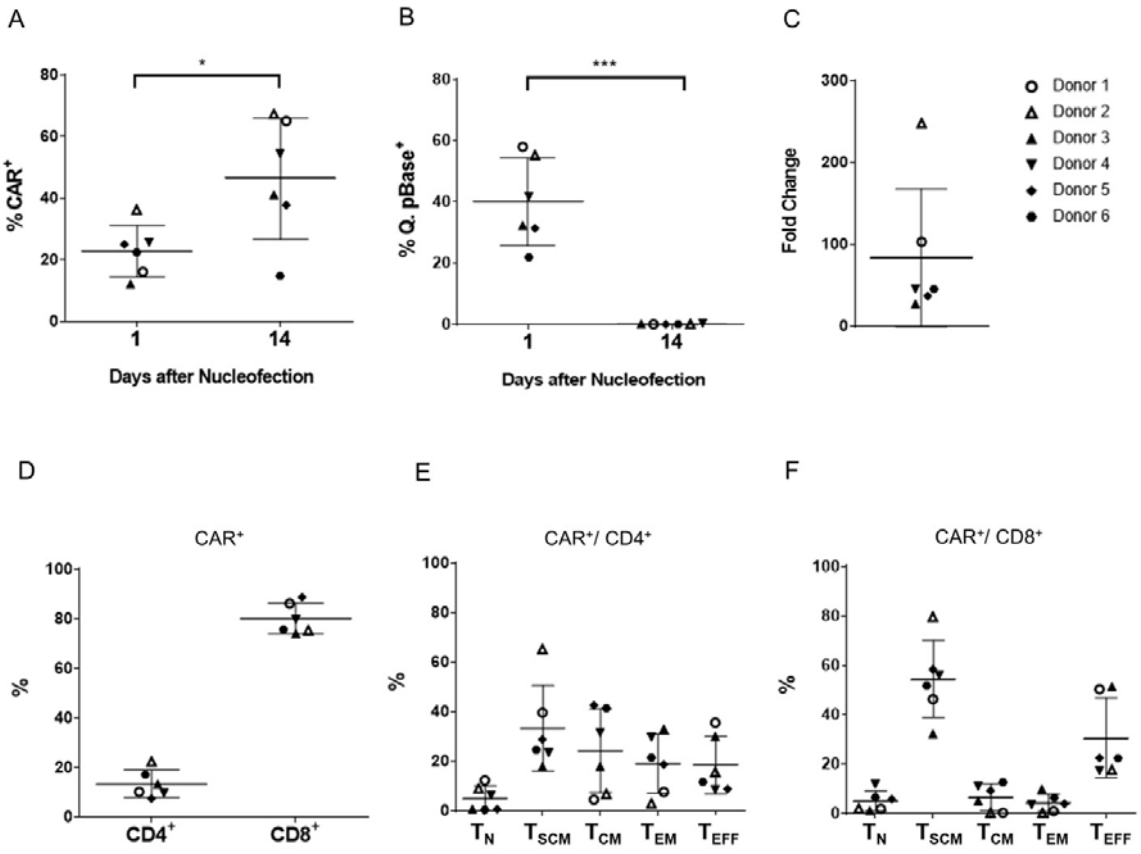

Figure 5. Characterization of healthy donor CAR-T cells produced using the *Qunatum pBac*™ (*qPB*) system

Percentages of (A) CAR^+ and (B) $transposase^+$ (*qPBase*$^+$) cells on days one and 14 following electroporation. (C) Fold expansion of cells after 14 days of culture. (D) Distribution of $CD4^+$ and $CD8^+$ T cell subtypes in CAR^+ T cells. Distribution of five T cell differentiation subsets T_N, T_{SCM}, T_{CM}, T_{EM} and T_{EFF} in (E) $CD4^+$ CAR^+ and (F) $CD8^+$ CAR^+ T cells on day 14. Results shown are from six healthy donors. Horizontal lines in (A, B, and D-F) represent the mean percentage of cells ± SD that are positive for the respective markers, and in (C) the mean fold change ± SD. * $p < 0.05$, *** $p < 0.001$. N = 6 PMBC donors.

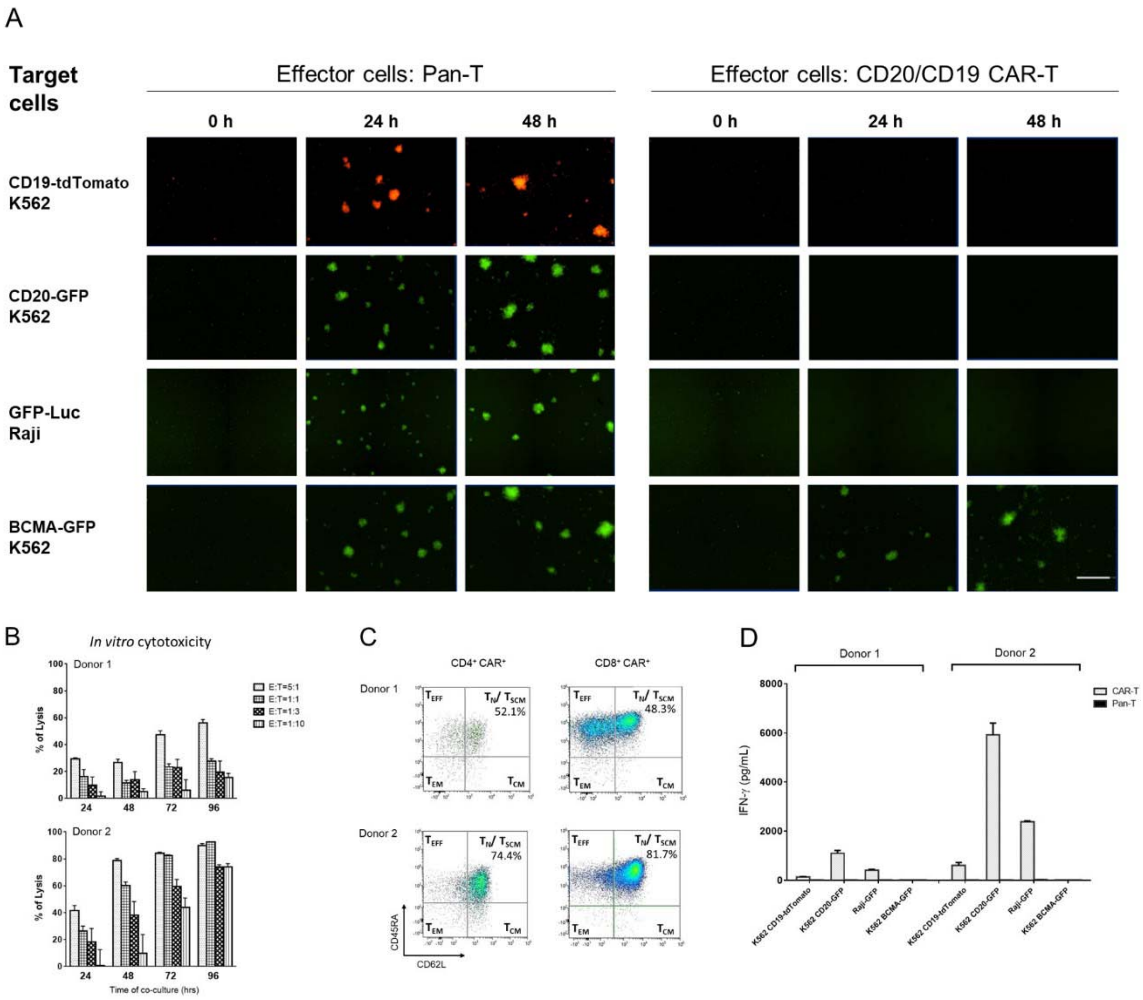

Figure 6. *In vitro* functional characterization of CAR-T cells produced using the *Qunatum pBac*™ (*qPB*) system

In vitro cytotoxicity results of Pan-T and/or CAR-T cells derived from healthy donor(s) (A) against the indicated target cells, and (B) at the indicated Effector: Target (E: T) ratio against Raji cells. (C) Representative flow cytometry data showing the distribution of T cell differentiation subsets T_N/T_{SCM}, T_{CM}, T_{EM} and T_{EFF} in $CD4^+$ and $CD8^+$ subtypes of donor 1 and donor 2 CAR^+ T cells. (D) IFN-γ secretion by donor 1 and donor 2 CAR-T cells following antigen stimulation. Pan-T cells (non-gene modified cells) served as a control group. Data shown in (B and D) represent the mean percentage of cell lysis ± SD and the mean IFN-γ concentration ± SD, respectively. N = 3 (triplicates). Bar in (A) represents 500 μm.

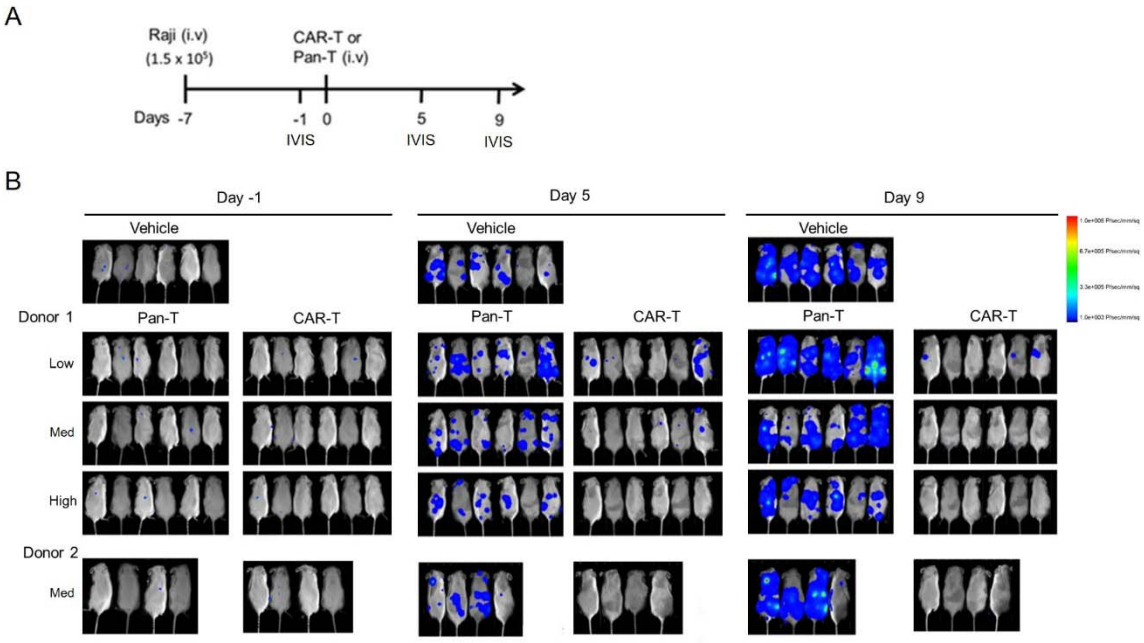

Figure 7. *In vivo* functional characterization of CAR-T cells produced using the *Qunatum pBac*™ (*qPB*) system in Raji-bearing immunodeficient mice

(A) A schematic depiction showing the design of the *in vivo* functional characterization experiment. (B) Bioluminescent imaging (IVIS) results showing the extent of tumor cell persistence one day prior to, and five and nine days following CAR-T or Pan-T cells injection. N = 4 or 6 mice/group.